

Concurrent application of conductive biopolymeric chitosan/ polyvinyl alcohol/ MWCNTs nanofibers, intracellular signaling manipulating molecules and electrical stimulation for more effective cardiac tissue engineering

Ali Abedi^{a,1}, Behnaz Bakhshandeh^{b,*}, Ali Babaie^{a,h,1}, Javad Mohammadnejad^{a,**}, Sadaf Vahdat^c, Reza Mombeiny^d, Seyed Reza Moosavi^e, Javid Amini^f, Lobat Tayebi^g

^a Department of Life Science Engineering, Faculty of New Sciences and Technology, University of Tehran, Tehran, Iran

^b Department of Biotechnology, College of Science, University of Tehran, Tehran, Iran

^c Tissue Engineering and Applied Cell Sciences Division, Department of Hematology, Faculty of Medical Sciences, Tarbiat Modares University, Tehran, Iran

^d Cellular and Molecular Research Center, Iran University of Medical Sciences, Tehran, Iran

^e Faculty of Pharmacy, Tehran University of Medical Sciences, Tehran, Iran

^f Department of Mechanical Engineering, Islamic Azad University, Science and Research Branch, Tehran, Iran

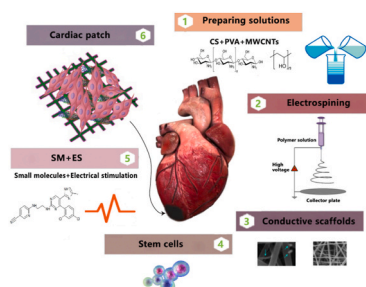
^g Marquette University School of Dentistry, Milwaukee, WI, 53201, USA

^h Department of Chemistry and Biotechnology, Faculty of Science Engineering and Technology, Swinburne University of Technology, Hawthorn, Victoria 3122, Australia

HIGHLIGHTS

- Electrospun scaffolds based on chitosan and different concentrations of MWCNTs were fabricated.
- Scaffold containing of MWCNTs (2% w/w) has most matching with the properties of extracellular matrix in cardiac tissue.
- Cardiac differentiation process was performed by using a 10-day electrochemical differentiation protocol.
- Over expression of cardiac-associated genes along with proper phenotypic alteration were observed.

GRAPHICAL ABSTRACT



ARTICLE INFO

Keywords:

Chitosan
Carbon nanotubes
Electrical stimulation
Small molecules
Unrestricted somatic stem cells
Cardiac tissue engineering

ABSTRACT

Fabrication of appropriate electro-conductive scaffold, application of small molecules (SMs), electrical stimulation (ES), and stem cells are steps forward in cardiac tissue engineering. Herein, for the first time, all mentioned factors have been taken into account concurrently regarding the differentiation of unrestricted somatic stem cells (USSCs) into cardiac cells. To accomplish this goal, electrospun composite scaffolds made of chitosan (CS) and polyvinyl alcohol (PVA) with multi-wall carbon nanotubes (MWCNTs; ranged from 0 to 2.5% w/w) were fabricated. After analyzing mechanical, electrical, and biological properties, the best MWCNTs portion was selected. Of note, the addition of 2%w/w MWCNTs to the CS/PVA samples reduced average fiber diameter from

* Corresponding author. Department of Biotechnology, College of Science, University of Tehran, 14155, Tehran, Iran.

** Corresponding author. Department of Life Science Engineering, Faculty of New Sciences & Technologies, University of Tehran, 14395, Tehran, Iran.

E-mail addresses: b.bakhshandeh@ut.ac.ir (B. Bakhshandeh), mohammadnejad@ut.ac.ir (J. Mohammadnejad).

¹ Authors have contributed equally in experimental work.

225 to 110 nm, increasing electrical conductivity from 8×10^{-5} S/m to 9×10^{-3} S/m and trebling tensile strength. Then, by using a 10-day differentiation protocol (including CHIR99021, IWP2, SB431542, and purmorphamine SMs) and ES, USSCs were induced into cardiomyocytes. Overexpression of some cardiac-associated genes, including troponin I, CX43, and β -MHC, along with proper phenotypic alteration, were observed. (Scaffold + SM + ES) show a significant increase in the expression of these genes, 172, 5.3, and 64-times as normalized to undifferentiated cells, respectively. Our findings confirmed the importance of the simultaneous implementation of different factors for the developing functionality of the cardiac tissue. Altogether, it is recommended to deploy all mentioned features to obtain effective cardiac tissue engineering.

1. Introduction

Cardiac diseases include 33–40% of all documented death causes [1, 2]. In 2008 alone, 17.3 m people have died of cardiac diseases, whereas in 2017, it increased to 17.8 m people [3,4]. It has been estimated that these diseases cost over 33 billion US dollars and 700 million UK pounds annually [5]. Tissue engineering is an emerging approach for the treatment of cardiac diseases, which does not have the drawbacks of other methods such as donor limitations, low efficiency, and high cost [6]. In this method, choosing the proper materials in scaffold fabrication, a suitable source of cells, and the method of cardiac differentiation are of high importance [7].

The first step in engineering of cardiac tissue is the fabrication of a biocompatible scaffold that mimics the electrical and mechanical properties and provides a proper environment for attachment and growth of cells, as well as ECM composition of the cardiac tissue [8–14]. Human left ventricular tissue has an electrical conductivity of 1.6×10^{-3} S cm⁻¹ and a thickness of around 1 cm. In terms of mechanical properties, the young modulus of the human ventricle is between 0.02 and 0.5 MPa [14].

Multi-wall carbon nanotubes (MWCNTs) have been shown promising conductive materials in biomedical engineering [15]. Compared to the other conductive polymers, MWCNTs have a better potential for increasing the mechanical properties and attachment of different chemical and biological functional groups [15,16]. Conductive scaffolds using MWCNTs have been extensively applied for cardiac tissue engineering [15–17]. Most of the previous works on MWCNTs have focused on the optimization of MWCNTs content on the biocompatibility of scaffolds [18,19]. In previous studies, adding carbon nanotubes to polylactic-co-glycolic acid (PLGA) (to make cardiac patch increased cardiac cell growth in the area of dead cardiac cells [20]. Moreover, the addition of 1 wt% MWCNTs to chitosan (CS)/PVA scaffolds was satisfactory in cardiac tissue engineering, and differentiated rat mesenchymal stem cells had high expression of cardiac cell markers compared to the control sample [19]. In this study, MWCNTs were used with CS/PVA composites to optimize mechanical and electrical properties in order to mimic the ECM of cardiac tissue. CS is a biocompatible natural polysaccharide with broad application in tissue engineering because of its biocompatibility, non-toxicity, hydrophilicity, rapid kinetics, and high processability [16, 21,22]. However, PVA was used to improve the spinnability of CS. PVA is a biocompatible water-soluble polymer that can be incorporated into composites with CS through electrospinning for tissue engineering applications [16,23].

The presence of electrical stimulations is an essential factor in the growth and maturation of osteoblasts, fibroblasts, and skeletal muscle, cardiac, and neural cells [24]. More specifically, for cardiac cells, controlled electrical stimulation, and mimicking the native cardiac environment are critical factors in maturation and functionality of cardiac cells and their beating behavior [25–27].

Aside from scaffold fabrication, optimization, and electrical stimulation usage, we have used small molecules, including CHIR99021 (CHIR), IWP2, SB431542, and purmorphamine, that induced cardiac differentiation of hESCs [28]. The influence of chemical factors, including small molecules on the differentiation of stem cells, is a well-established area [28,29]. Unrestricted somatic stem cells (USSCs)

were chosen to study cardiac differentiation. This class of stem cells reside in an early differentiation state and can produce endodermal, ectodermal, and mesodermal cells without any ethical concerns [30,31]. Given the potential to differentiate into different cell lines, the usage of these cells for *in vitro* and *in vivo* research is recommended [30,32].

The aim of this research is to gather most of the influential and recommended factors to achieve more efficient cardiac tissue engineering. First, fabrication and optimization of the properties of scaffolds close to the extracellular matrix of cardiac tissue were performed. Then, simultaneous application of optimized conductive scaffold, electrical stimulation, and small molecules for cardiac differentiation of USSCs were considered for the first time. Finally, the altered expression of some cardiac gene markers was evaluated to investigate the possible cardiac differentiation.

2. Materials and methods

2.1. Materials

DMEM, FBS, Trypsin/EDTA, PBS, RPMI 1640, B27 without insulin, and Penicillin/Streptomycin were purchased from Gibco (USA). DMSO, trypan blue, ethanol, glutaraldehyde, and hydrolyzed PVA were purchased from Merck (Germany). MTT powder, SB431542, and CS (medium molecular weight) were purchased from Sigma (USA). CHIR and purmorphamine were purchased from Stemgent (USA). 5-Azacytidine, carboxyl-functionalized MWCNTs, and IWP2 were purchased from Santa Cruz (USA), Neutrino (Iran) and Tocris Bioscience (UK) respectively.

2.2. Scaffold fabrication and characterization

2.2.1. Preparation of solutions

CS (4%w/v) was dissolved in acetic acid solution (7%v/v) on a stirrer at room temperature. Aqueous PVA solution (12%w/w) was prepared by dissolving PVA in deionized water on stirrer at 80 °C. After cooling down, CS and PVA solutions were mixed by stirring at 200 rpm at room temperature for an hour. In order to make scaffolds with different MWCNTs contents (0, 0.5, 1, 1.5, 2 and 2.5%w/w), MWCNTs were added into CS/PVA solution and dispersed using water bath sonication and homogenizer at 10,000 rpm for 10 min each. Subsequently, the mixture was stirred for another 72 h at 200 rpm at room temperature for further homogenization. The amount of MWCNTs required for each of the scaffolds was determined based on the dry content of MWCNTs and CS/PVA. Before electrospinning, the conductivity of electrospinning solutions was measured using an electrical conductometer (WPA-CMD, UK) at room temperature five times, and the results are presented in Table 1 (average \pm standard deviation).

2.2.2. Fabrication of nanofibrous scaffolds

After preparing the solutions, they were loaded into 5 ml syringes and placed into an electrospinning device (Nanoazma, Iran). Electrospinning was completed using a dual-nozzle setup with 23-gauge needle, 0.3 mL/h flow rate at each needle, 16 cm needle-to-drum distance, and 25 KV. The drum (5 cm in diameter) was covered with aluminum foil and rotated at 800 rpm. After completion of electrospinning, spun sheets

Table 1
Details of content and electrical conductivity of electrospinning solutions.

Sample	CS: PVA	MWCNT (wt. %)	Electrical conductivity of electrospinning solution ($\mu\text{S}/\text{cm}$)
CS/PVA	1:3	0	240 ± 51
CS/PVA/ MWCNT (0.5)	1:3	0.5	1070 ± 39
CS/PVA/ MWCNT (1)	1:3	1	1090 ± 11
CS/PVA/ MWCNT (1.5)	1:3	1.5	1140 ± 18
CS/PVA/ MWCNT (2)	1:3	2	1176 ± 29
CS/PVA/ MWCNT (2.5)	1:3	2.5	1074 ± 42

were removed from aluminum foil. Then, electrospun sheets were placed in a desiccator and cross-linked using glutaraldehyde vapor from a solution of 0.2 M glutaraldehyde + 1%v/v HCl at 80 °C for 1 h. Samples were then placed in a vacuum oven overnight to remove any remaining vapors. Residual glutaraldehyde was removed using 1% w/v aqueous glycine solution for 15 min. Scaffolds were sterilized using 70% ethanol before cell culture [76].

2.2.3. Scaffold characterization

Scaffolds were cut into 20 mm \times 10 mm pieces and morphology of them was imaged using a scanning electron microscope (SEM; HITACHI S-4160, Hitachi, Japan). The diameter of fibers was calculated using the Image J software (Image J, National Institutes of Health, USA). The topographical images (20 mm \times 10 mm pieces) were obtained using a scanning laser microscope (Olympus OLS4100, Olympus Corporation, Japan). Surface topography was analyzed using OLS4100 offline V3.1.1 software (Olympus Corporation, Japan) [9]. Porosity percentage of the scaffolds were evaluated by using the Python 3.8.0 software and SEM images of samples [33].

The mechanical properties of the scaffolds were measured through universal tensile testing (Instron-3367). Scaffolds were cut into 30 mm \times 5 mm pieces and fixed in grips. Minimum of 3 samples was tested from each scaffold and tensile strength; Young modulus and strain at the point of the break were measured [9].

The electrical conductivity of cross-linked scaffolds was measured using Keithley Multimeter (Keithley-2361, Keithley Instruments, USA). Electrospun sheets with 50 μm of thickness were placed into the 1 cm gap between two electrodes. By applying a voltage range between -10 and 10 KV with 0.2 KV resolution, the current was recorded, and the conductivity values were calculated [9].

The static contact angle of the scaffolds was determined using an angle measuring device (OCA 15 plus – Dataphysics, Germany). For this purpose, samples were cut into 30 mm \times 10 mm pieces, a 4 μL drop of water was placed on the surface of the scaffolds at standard ambient temperature, and the contact angle values were calculated. For each sample, the experiment was repeated three times. The obtained values were reported as the mean of contact angle with standard deviation [76].

In order to assess the chemistry of scaffolds, dry scaffolds have been crushed into powder and compressed into pellets using KBr powder. Then, samples were analyzed using an FTIR device (L1280032-frontier, Perkin Elmer, USA) [76].

2.3. Stem cell culture and cell/scaffold attachment analysis

USSCs were provided from the stem cell research center in Tehran, Iran. Cells were cultured in DMEM, 10% FBS and 1% Penicillin/Streptomycin (culture medium) in incubator at 37 °C, 90% humidity and 5% CO₂. Media was changed every 2–3 days, and upon 70–80% of confluence, cells were sub-cultured into new flasks using trypsin/EDTA.

Cell attachment assay was carried out to evaluate the cell-scaffold

interactions. Scaffolds were punched (10 mm \times 5 mm pieces) and placed at the bottom of the 12-well plates. Scaffolds were sterilized using 70% ethanol solution for 2 h followed by triple PBS wash. 20,000 cells were seeded on each scaffold, as well as in tissue culture plastics (TCPs). Cells were cultured for 24 h before fixation for SEM. Afterward, cells were washed with PBS to remove any debris and dead cells. Then, cells were fixed using 2.5%v/v glutaraldehyde solution in PBS for 3 h. Finally, water content was excreted using ethanol washing steps (60, 70, 80, 90, and 100%v/v 15 min each). Cells were imaged using SEM (HITACHI S-4160, Hitachi, Japan) [76].

2.4. Cytotoxicity analysis

For cell toxicity assessment of the fabricated scaffolds, the metabolic activity of cells on scaffolds was assessed using MTT assay. Scaffolds were prepared (10 mm \times 5 mm pieces), and cells were seeded similar to cell attachment assay. MTT assay was performed at days 1, 3, and 7. In brief, cells were incubated for 4 h with 0.5 mg/mL MTT dissolved in culture medium (500 μL). Afterward, the medium was removed, and cells were washed with PBS to remove any debris. Formazan was dissolved into 200 μL of DMSO, and optical densities of formazan were measured at 540 nm [9].

2.5. Induction of cardiac differentiation using small molecules and electrical stimulation

Scaffolds (10 mm \times 5 mm pieces) were placed at the bottom of 12-well plates and were seeded by USSCs at a density of 2×10^5 cells/well. In this section, RPMI-B27 culture medium (RPMI 1640 + 2% B27 without insulin + 1% penicillin) was used. The studied groups and the used treatments are listed in Table 2. Differentiation was induced using a 10-day induction protocol, as illustrated in Fig. 1. In brief, at zero point after cells seeding, 5-azacytidine (20 $\mu\text{L}/\text{mL}$) was used with RPMI medium for 24 h. On day 1, the media was replaced by culture media containing CHIR (12 μm). At day 2, media was replaced with fresh media containing IWP2, SB431542, and purmorphamine (5 μm each) for 2 days. After that, the medium was changed every 2 days until the end of the protocol [28]. Electrical stimulation was applied at the start of day 8 for 48 h using a pulse generator device (GPS-2105 function generator, General Polytronic System Ltd, UK). Monophasic pulses were applied at 1.25 Hz of frequency and 10 V of voltage for 2 cm-long scaffolds.

2.6. Gene expression analysis

In order to evaluate the gene expression pattern of differentiated cells on scaffolds, RNA was extracted at the end of day 10, and cDNA was synthesized. Gene expression analysis was carried out by qPCR assay using primers listed in Table S1 for the cardiac gene markers, including cardiac troponin I (cTnI), CX43, α -MHC and β -MHC, and β 2M as the housekeeping gene.

Table 2
Different differentiation study groups and their treatments.

Samples	Scaffold	Small molecules	Electrical stimulation (ES)	Named as
USSCs on TCP	–	+	–	TCP
USSCs on scaffold	+	+	–	Scaffold + SM
USSCs on scaffold	+	+	+	Scaffold + SM + ES
USSCs on TCP	–	–	–	Control

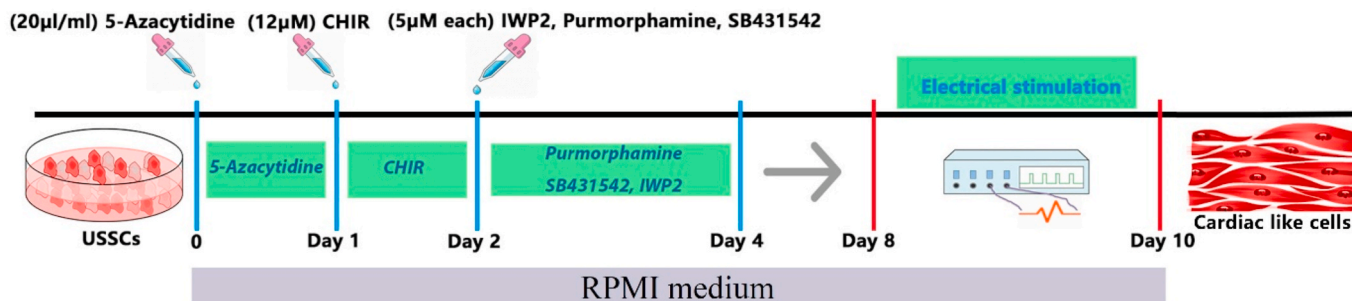


Fig. 1. Infographics of the 10-day differentiation protocol used for differentiation of USSCs into cardiomyocyte-like cells. The media was changed every 48 h.

2.7. Statistical analysis

The data is presented as mean \pm standard deviation. Statistical analysis was assessed using a *t*-test, considering p -value ≤ 0.05 as statistically significant [76]. For each sample, the tests were repeated at least three times.

3. Results and discussion

3.1. Scanning electron microscopy and fiber diameter analysis

The diameter of electrospun fibers depends on several parameters, including concentration and electrical conductivity of electrospinning solution [34]. Adding MWCNTs to CS/PVA scaffolds intensifies the solid content of solutions and the concentration of electrospinning solution, which in turn results in the formation of thicker fibers [35–37]. However, adding conductive MWCNTs particles to electrospinning solution intensifies the stretching of fibers during electrospinning, which leads to the formation of thinner fibers [9,34]. As presented in Fig. 2 and Fig. 3, the supplementation of MWCNTs to CS/PVA scaffolds results in thinner

fibers. In the CS/PVA/MWCNT (0.5) sample, which has the lowest MWCNTs, the average diameter of the fibers decreases from 226 to 157 nm. The maximum decrease in fiber diameter is observed in the CS/PVA/MWCNT (2) sample, reduced to 114 nm. As shown in Table 1, by adding 2 wt% MWCNT to PVA/CS solutions, conductivity is increased by 5 times, which results in decreasing the fiber diameter by 3 times compared to the CS/PVA sample. In this regard, Avinash Baji et al. reported that a 32-fold increase in the electrical conductivity of an electrospinning solution could lead to a 10-fold decrease in the average diameter of the fibers [34].

As CS/PVA and CS/PVA/MWCNT (2) samples were treated in the same electrospinning conditions, the only electrospinning parameters affecting the fiber diameter might be concentration and electrical conductivity. By adding MWCNTs to CS/PVA solutions, the concentration of the electrospinning solution will increase. However, as the thickness of fibers is decreased, the impact of electrical conductivity is probably more dominant than concentration. Similar studies on conductive polymers and scaffolds containing MWCNTs and other conductive polymers have also shown that higher conductivity will result in thinner fibers [9,34]. According to a research, the addition of 0.55 wt%

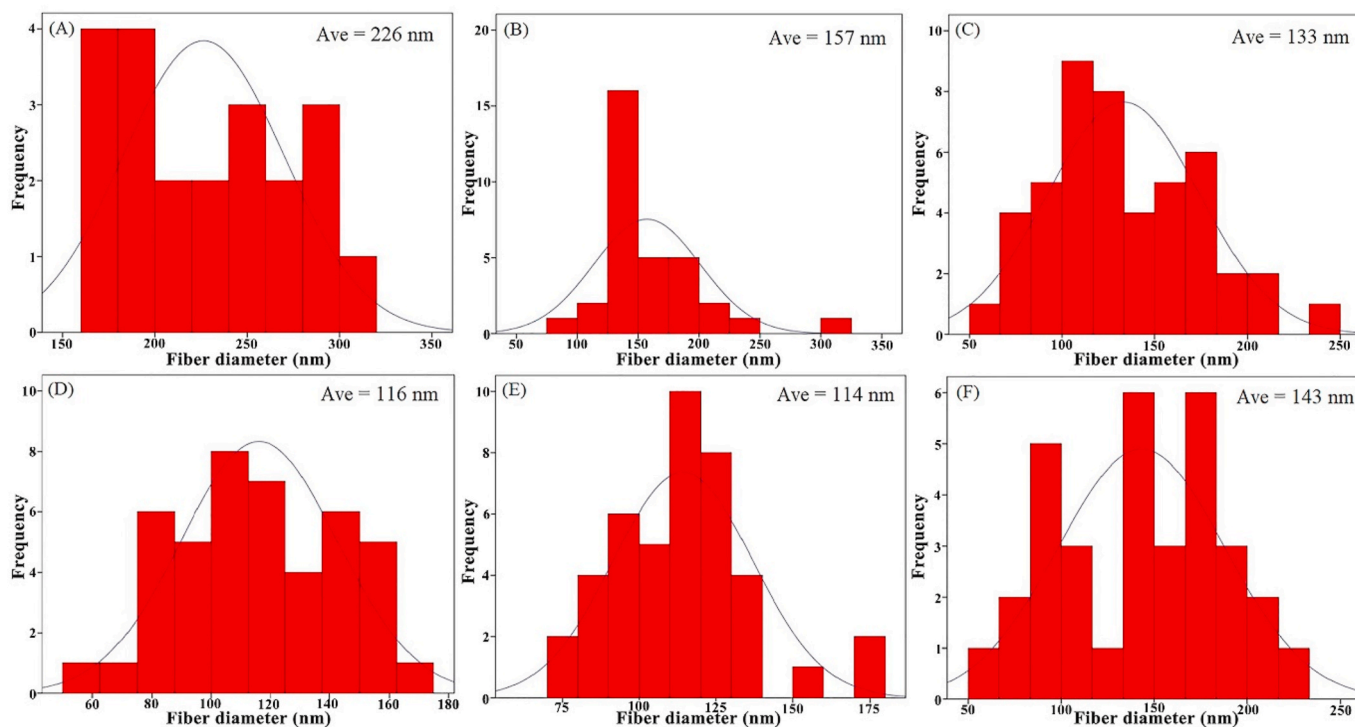


Fig. 2. Fiber diameter of different scaffolds with fiber distribution data: A: CS/PVA, B: CS/PVA/MWCNT (0.5), C: CS/PVA/MWCNT (1), D: CS/PVA/MWCNT (1.5), E: CS/PVA/MWCNT (2) and F: CS/PVA/MWCNT (2.5). As presented, adding MWCNTs up to 2 wt% resulted in reduction of fiber diameters. The differences between fiber diameter of all MWCNT-incorporated samples compared to the CS/PVA sample were statistically significant (p -value less than 0.05).

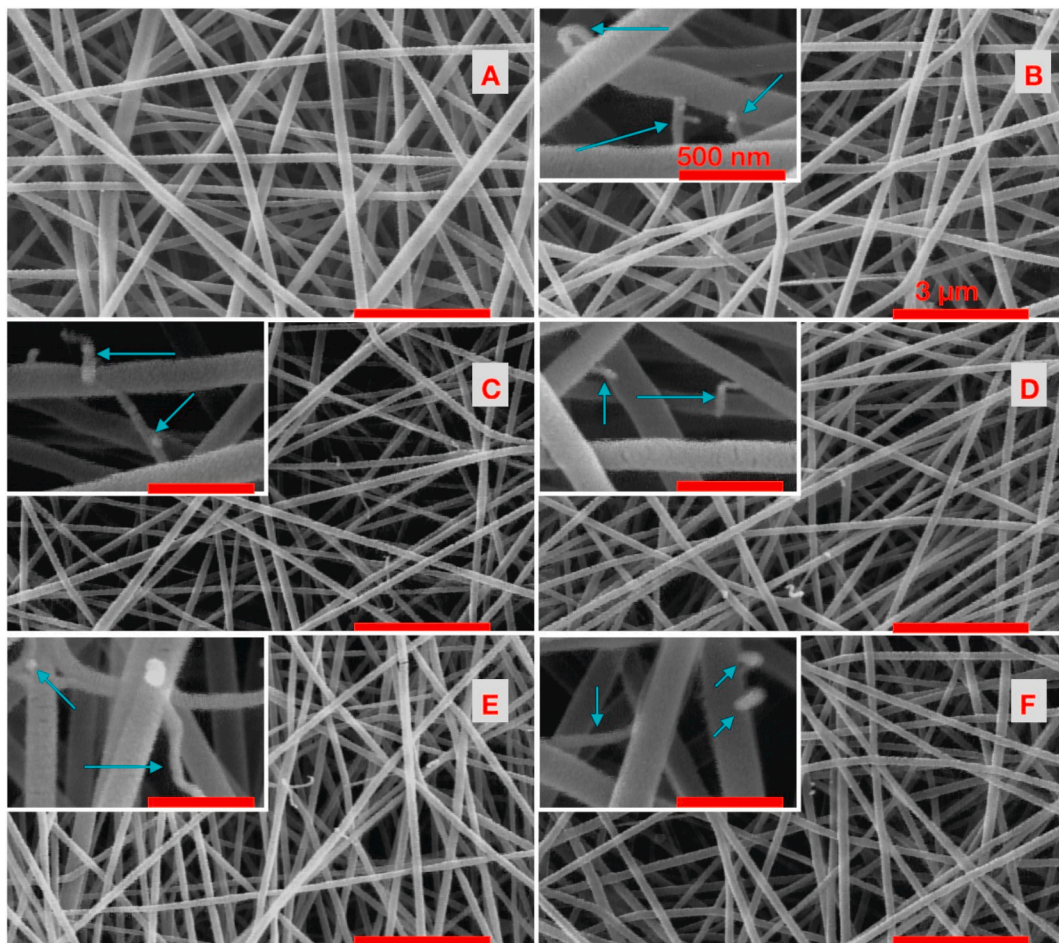


Fig. 3. SEM images of fabricated scaffolds: A: CS/PVA, B: CS/PVA/MWCNT (0.5), C: CS/PVA/MWCNT (1), D: CS/PVA/MWCNT (1.5), E: CS/PVA/MWCNT (2) and F: CS/PVA/MWCNT (2.5). Scale bars in large and small images equal to 3 μ m and 500 nm, respectively. MWCNTs are indicated with arrows in the small images. As mentioned earlier, increasing the amount of MWCNTs in the samples leads to a decrease in the mean diameter of the fibers.

MWCNTs to the cellulose in the electrospinning process resulted in a decreased in mean fiber diameter from 321 to 228 nm [38]. In this regard, adding 3 wt% MWCNTs in ethylene vinyl acetate (EVA) reduces the average diameter of the fibers from 2504 to 846 nm; this finding is in congruence with the previous report due to the amplified electrical conductivity of the electrospinning solution [39]. The results related to the porosity of the samples are also presented in Table 3. The porosity percentage in all samples is almost close to each other. The highest porosity were in CS/PVA/MWCNT (0.5), CS/PVA/MWCNT (1), and CS/PVA/MWCNT (1.5) samples, but these results were not significant compared to each other. The similarity of these values is probably due to

the fact that all samples are cross-linked by glutaraldehyde in the same way.

3.2. FTIR analysis

In order to assess the existence of chemical functional groups in fabricated scaffolds, samples were evaluated using the FTIR method (Fig. 4). Considering the low content of MWCNTs in scaffolds, which varies between 0.5 and 2 wt%, nuance changes in FTIR results are expected. On the other hand, both CS and PVA have several peaks of C–H and O–H, which overlap the peaks associated with MWCNTs [9,40].

Table 3

Mechanical properties (indicated by Young's modulus, elongation at break and ultimate strength), electrical conductivity, porosity percentage, and static contact angle of different electrospun scaffolds.

Sample	Young's Modulus (MPa)	Elongation at break (%)	Ultimate strength (MPa)	Electrical conductivity (S/m)	Porosity percentage (%)	Static Contact Angle (deg)
CS/PVA	275	6.5 ± 0.1	9.9 ± 0.52	$10^{-5} * 8$	29 ± 2	41.56 ± 1.82
CS/PVA/MWCNT (0.5)	399	6.1 ± 0.3	13.7 ± 0.46	$10^{-3} * 1.56$	32 ± 2	29.89 ± 1.05
CS/PVA/MWCNT (1)	774	4.4 ± 0.1	16.1 ± 0.81	$10^{-3} * 5.9$	31 ± 3	26.47 ± 1.44
CS/PVA/MWCNT (1.5)	830	3.4 ± 0.2	22.1 ± 1.05	$10^{-3} * 6.94$	31 ± 4	24.36 ± 0.72
CS/PVA/MWCNT (2)	941	3.8 ± 0.2	30 ± 1.74	$10^{-3} * 9$	29 ± 3	23.78 ± 0.77
CS/PVA/MWCNT (2.5)	733	2.2 ± 0.1	12.9 ± 1.39	$10^{-3} * 1$	27 ± 1	26.19 ± 2.1

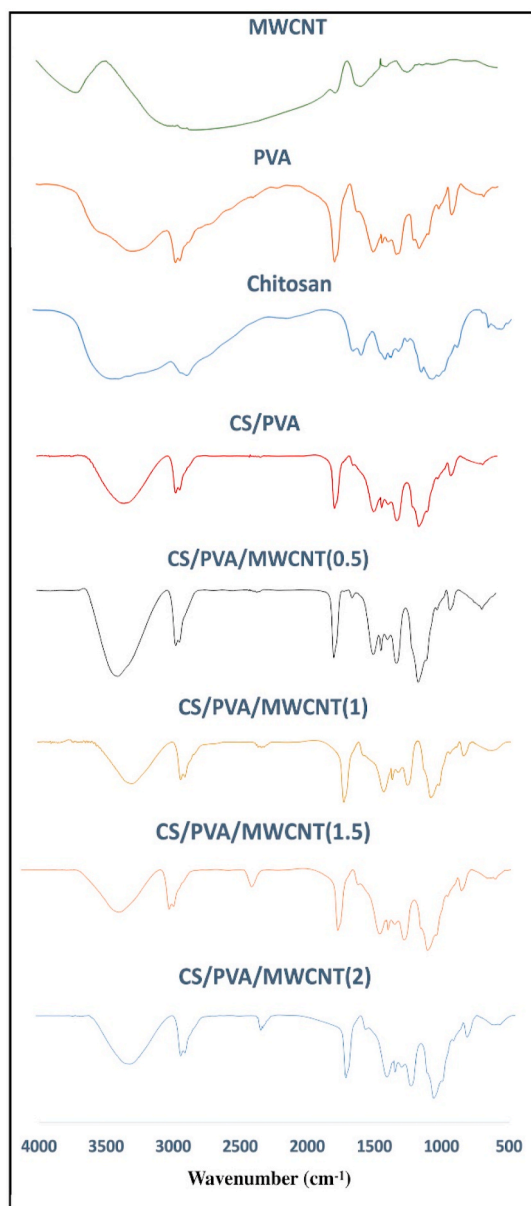


Fig. 4. FTIR spectrum of all fabricated scaffold samples. As mentioned earlier, with the addition of MWCNTs to the samples, a peak appears in the approximate range of 2350 wave number. Due to the abundance of CS and PVA peaks in the range of 3000–3500 wave number, peak separation will be difficult for each sample within this range.

Therefore, MWCNTs, CS, and PVA samples were tested solely to determine their chemical functional groups in detail.

In Fig. 4, the largest peaks are related to stretching of O–H in CS at 3335, 3376, 3384 cm^{-1} , according to the previous reports [40–42]. The other significant peaks at 2941 and 2943 cm^{-1} are related to stretching of C–H in PVA and CS, however, these peaks are more distinct in PVA [40,41]. Another large peak at 1737 cm^{-1} in PVA might be related to remaining vinyl alcohol monomers from the hydrolysis process [9]. This peak exists in all scaffolds with a small shift at 1734 and 1735 cm^{-1} . Peaks at 1380 cm^{-1} for CS and 1446 cm^{-1} in PVA are related to bending of C–H [42], which are obvious in scaffold samples with peaks at 1375–1377 cm^{-1} and 1435–1437 cm^{-1} , respectively. The peak at 1656 cm^{-1} is related to N–H in the chitin of CS, and the C–N functional group of acetyl group in chitin is observable at 1259 cm^{-1} [9]. The only detectable peak related to MWCNTs is observable at 2357 cm^{-1} , which is more distinct in samples with higher MWCNTs content. This peak,

which might be related to C–O bonds in the carboxyl group, was not observed in samples without MWCNTs [43].

3.3. Mechanical properties of the scaffolds

Mechanical properties of electrospun scaffolds, as well as details on Young modulus, ultimate tensile strength, and strain breakpoint, are presented in Table 3. Other reports on MWCNTs have shown that adding MWCNTs will result in enhanced mechanical properties of scaffolds due to the superior mechanical strength of MWCNTs. Young modulus and tensile strength of MWCNTs range from 270 to 950 GPa and 11–62 GPa, respectively [44]. In this research, increasing the MWCNTs content of scaffolds results in enhanced mechanical properties of scaffolds until the point where the dispersion of MWCNTs is disrupted due to the high content of MWCNTs and their possible agglomeration. As an example, adding 1 wt% MWCNTs to CS/PVA scaffolds results in an increase in tensile strength from 9.9 MPa to 16.1 MPa. The maximum enhancement of mechanical properties is observed in CS/PVA/MWCNT (2) scaffolds, where as compared to CS/PVA scaffolds, a 3-fold increase in both ultimate tensile strength and young modulus was observed.

However, adding 2 wt% of MWCNTs has also resulted in increased brittleness of scaffolds, shown by 42% decrease in strain at the point of failure. Overall, in all scaffold samples, adding MWCNTs have resulted in higher tensile strength and lower strain at the point of the break. The enhanced tensile strength of scaffolds might be the result of two main factors: a decrease in fiber diameter and strong bonds in the MWCNT-CS interface [9,45,46].

In thicker fibers, due to higher crystalline defects, stretching of fibers occurred with a lower amount of force, which resulted in a decrease of Young modulus and tensile strength (Table 3). In contrast, thinner fibers had a better formation of polymeric chains with lower defects [9,45,47]. In another research, adding PEDOT to CS/PVA scaffolds has resulted in a decrease in fiber diameter from 144 nm to 83 nm, which resulted in increasing tensile strength from 9 MPa to 18 MPa [9]. Figs. 2 and 3 show that scaffolds with higher amounts of MWCNTs have thinner fibers, which in turn enhance their mechanical properties. For instance, CS/PVA/MWCNT (2) with the lowest fiber diameter, shows the best mechanical properties.

Aside from fiber diameters, MWCNTs can interact with the carrier polymers like the other polymeric nanocomposites. If we ignore the weak van der Waals links as well as the entanglement between MWCNTs and CS, there can be strong covalent chemical bonds between the two. Since CS contains many amino and carboxyl groups, it can form strong hydrogen bonds with functionalized MWCNTs. These bonds will be highly effective in enhancing the mechanical properties of composite [46–48]. In nanocomposites, particles with a large surface to volume ratio have an improved interaction between particles and carrier. Therefore, MWCNTs can be very effective in improving the mechanical properties of nanocomposites because of their large surface to volume ratio. For this reason, MWCNTs are being used to improve the mechanical properties of nanocomposites. For instance, in a similar study for cardiac tissue engineering, adding 1 wt% of CNTs to CS/PVA resulted in a doubling of the tensile strength and a 4-fold increase of the Young modulus [19]. In another study, adding 1 wt% MWCNTs into the CS matrix increased the tensile strength and elastic modulus by 33% and 47%, respectively [49]. High amount of MWCNTs in CS/PVA/MWCNT (2.5) sample likely results in agglomeration of particles due to van der Waals forces, which might act as defect points in the structure of fibers. The agglomeration might have decreased the conductivity of the electrospinning solution, resulting in thicker fibers, which may be another reason for lower mechanical properties [9,50]. In addition, the presence of other components in the chitosan structure, increases crystallinity and enhances mechanical properties [18,51]. Interactions between the amine groups present in chitosan with the carboxyl group in MWCNTs [51], hydroxyl group in polyvinyl alcohol, and aldehyde group in glutaraldehyde can increase the crystallinity of the scaffolds and

improve the mechanical properties and stability of fibers [52].

3.4. Conductivity of the scaffolds

In order to measure the electrical conductivity of electrospun fibers, scaffolds were cut in a way that the distance between the electrodes/surface area (L/A) of all samples remained constant. The I–V curve of all samples, as shown in Fig. 5, were plotted using a Keithley Instruments multimeter, and after that, the resistance of each scaffold was measured. The conductivity of scaffolds (σ) was measured using Eq. (1), and results are presented in Table 3.

$$\sigma = \frac{L}{R \cdot A} \quad (1)$$

where L is the distance between two electrodes, A is the cross-sectional area of the scaffolds; R is the resistance of scaffolds, collected from the I–V curve.

The usage of an electroactive scaffold is a suitable tool to electrically stimulate stimuli-responsive cells [53,54]. Electroactive scaffolds have an electrical conductivity higher than 10^5 S/m [53]. Most biodegradable polymers used in cardiac tissue engineering lack proper electrical properties. As presented in Table 3, although CS/PVA scaffolds lack proper electroactive properties, CS/PVA/MWCNT scaffolds were modified into electroactive scaffolds. CS/PVA/MWCNT (1), CS/PVA/MWCNT (1.5) and CS/PVA/MWCNT (2). Samples have approximately 100-fold higher electrical conductivity than the CS/PVA sample. More than being just electroactive, mimicking the electrical properties of the target tissue can highly direct cells into differentiation [9]. The conductivity of the native myocardium ranges from 1.6×10^{-1} S/m (longitudinally) to 5×10^3 S/m (transversally) [54,55]. These values are quite close to the electrical conductivity presented for scaffolds containing MWCNTs in Table 3, especially the CS/PVA/MWCNT (2)

sample (9×10^3 S/m), which is the highest among the other samples.

In a similar study that investigated the effect of electrical stimulation on mesenchymal stem cells, CS/PVA scaffolds containing 1 wt% of MWCNTs with 3.4×10^{-4} S/m conductivity have been described as satisfactory for cardiac tissue engineering [19]. Consistently, adding 1 wt% PEDOT:PSS to CS/PVA increased the conductivity of pure CS/PVA from 6×10^{-5} S/m to 7.6×10^{-3} S/m, of which the latter is a proper conductivity value for neural and cardiac tissue differentiation [9]. As the amount of MWCNTs in the samples increases, they become more difficult to dissolve. The agglomeration of MWCNTs particles reduces their possible contact in the scaffold network and results in a loss of electrical conductivity, as seen in the results for CS/PVA/MWCNT (2.5) [19]. However, CS/PVA/MWCNT (2) sample appears to be suitable for electrical stimulation in cardiac tissue engineering.

3.5. Static contact angle

The results for the contact angle values of the samples are presented in Table 3. The contact angle is decreased in all samples containing MWCNTs compared to CS/PVA samples. Adding 0.5 wt% MWCNTs to the CS/PVA sample reduces the contact angle from 41.56° to 29.89° . As presented in Fig. 6, the highest decrease is seen in CS/PVA/MWCNT (2) compared to CS/PVA samples, which is 34%. These may be associated with the presence of MWCNTs.

Carbon nanotubes as extraordinary mass transport channels are known to have high specific surface area [56,57]. The presence of functionalized types of them, in combination with the scaffolds, especially with the hydroxyl and carboxyl groups, are highly effective in enhancing the hydrophilicity of surfaces and reducing the contact angle [19,56,57]. In fact, the presence of carbon nanotubes in the CS/PVA compound increases the hydrogen bonds [19]. This, in turn, leads to more water molecule adsorption and reduction of the contact angle [19,

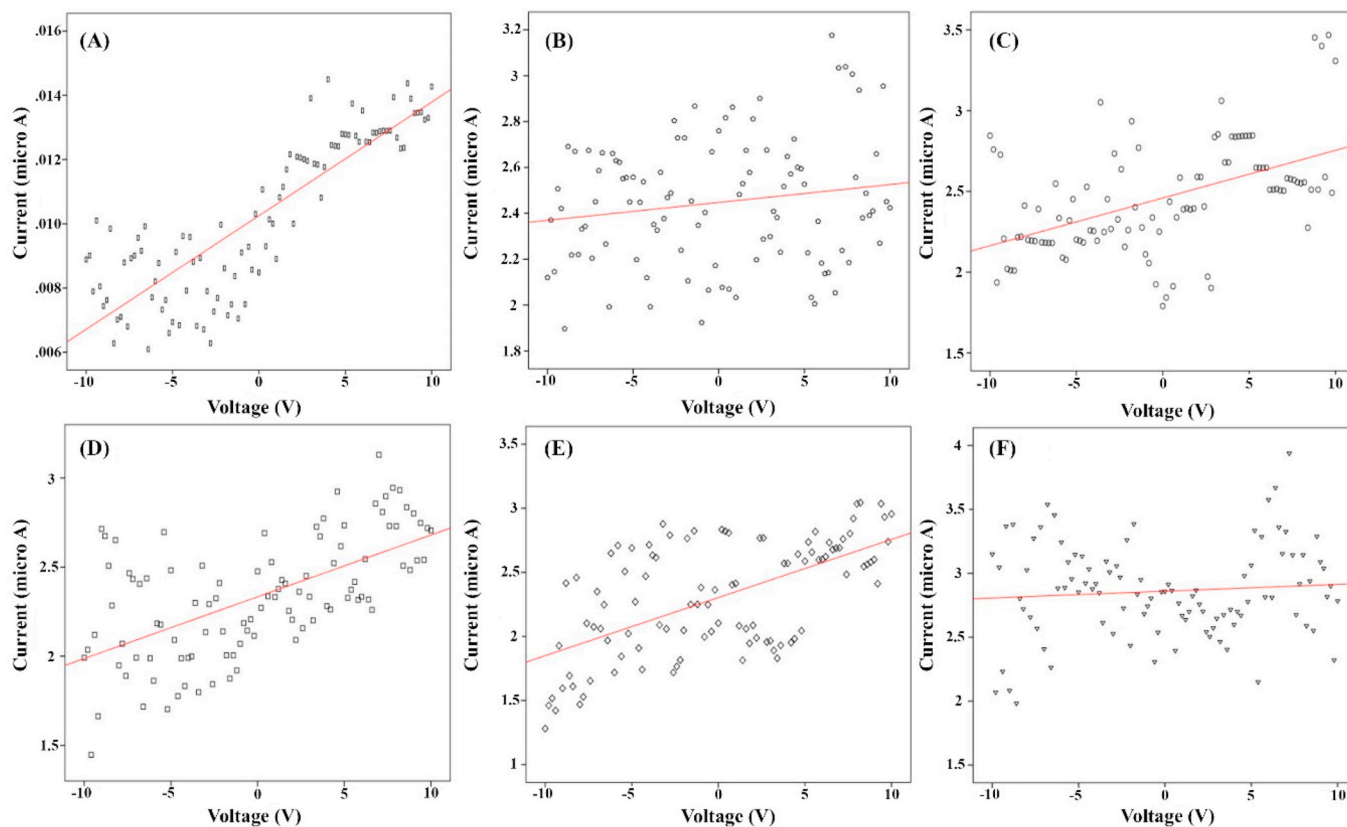


Fig. 5. The current-versus-voltage curve of scaffolds: (A): CS/PVA, (B): CS/PVA/MWCNT (0.5), (C): CS/PVA/MWCNT (1), (D): CS/PVA/MWCNT (1.5), (E): CS/PVA/MWCNT (2), (F): CS/PVA/MWCNT (2.5).

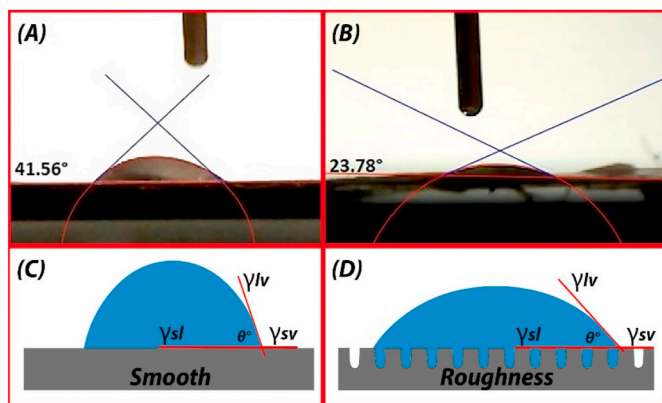


Fig. 6. Static contact angle images of water droplets on scaffolds: (A): CS/PVA, (B): CS/PVA/MWCNT (2). The addition of 2 wt% MWCNTs to the pure sample results in the maximum decrease in contact angle (p -values ≤ 0.05) compared to other samples.

[47,48]. On the other hand, the use of the ultrasonic method when dissolving MWCNTs in CS/PVA also removes the air barrier layers around the carbon nanotubes, causing them to not to agglomerate and increases their adsorption efficiency [58]. Also, according to the Wenzel theory (Eq. (2)), the amount of contact angle will be reduced with the presence of surface grooves and roughness factors in hydrophilic surfaces [59–61]. As shown in Fig. 6, surfaces with more roughness compared to smooth surfaces, lead to higher values of r index (ratio of the real contact area to the projected surface area) in Eq. (2), which will reduce the contact angle [59,61]. In this respect, Mombini et al. have reported that adding 1 wt% of functionalized CNTs to CS/PVA, leads to a 20% increase in water adsorption [19]. Remarkably, our data are in line with the results of previous studies. For instance, in Polyacrylonitrile (PAN), the addition of 2 wt% MWCNTs reduced the contact angle value from 50° to 42° [57]. In another study, the presence of 1 wt% MWCNTs reduced the contact angle value by 20% compared to the pure sample [56].

$$\cos\theta = \frac{\gamma_{sv} - \gamma_{sl}}{\gamma_{lv}} * r \quad (2)$$

where r is the ratio of the real contact area to the projected surface area, γ_{sl} is surface energies of solid-liquid, γ_{sv} is surface energies of solid-gas, γ_{lv} is surface energies of liquid-gas.

3.6. Evaluation of cell viability and attachment

In order to evaluate the influence of physical and chemical properties of the scaffolds on viability, metabolic activity and proliferation of USSCs, cells were cultured for 7 days on fabricated scaffolds. MTT assay and cellular attachment analysis were performed (Fig. 7 and Fig. 8).

Cellular attachment and proliferation depend on culture time, topographical features of the surface, and functional groups present on the surface of scaffolds [62]. By the end of the first day of culture, CS/PVA samples yield a higher number of cells than the MWCNTs-containing samples (p -values ≤ 0.05). As shown in Table 4, the surface and linear roughness of all MWCNTs-containing scaffolds are larger than CS/PVA samples. For instance, surface and linear roughness of CS/PVA/MWCNT (2) sample is 25% and 50% larger than CS/PVA samples. However, cell adhesion and viability are higher in the early hours of the first day on samples containing MWCNTs. In this regard, Hirada et al. have reported a better spreading and morphology on MWCNT-coated PLLA scaffolds 2 h after seeding as compared to control samples [63]. Upon seeding, cell attachment highly depends on the surface topography of the substrate. After the attachment phase, the critical factor in determining the viability and proliferation of cells is the chemical composition of scaffolds.

At the end of the first day and in the attachment phase, low cell survival rate on MWCNTs-containing scaffolds is observed, which may be related to two major factors. The first factor is the propulsion between the negative electrostatic charge of MWCNTs and the negative charge of the cell membranes. In a similar study, it was shown that adding 1 wt% of MWCNTs to CS/PVA scaffolds decreased the survival rate of fibroblasts by half in the first 24 h of culture [16]. Liu et al. showed that cell survival in the first 8 h of culture on PLGA/MWCNT scaffolds is 20% more than control samples. However, by the end of the first 24 h, the cell survival rate on MWCNTs-containing scaffolds has decreased compared to controls samples [64].

The other factor potentially affecting the low survival rate on the first day of culture is the chemical properties of MWCNTs. Functionalized MWCNTs, especially, can adsorb serum proteins on their surface, and subsequent decrease in the serum culture medium can lead to increased cell death [19,65]. On the other hand, CNTs can enter the cell membranes, whereas it is difficult for MWCNTs to enter the cell membranes due to their high diameter. The second cell entrance mechanism for CNTs is endocytosis, where colonies of these particles and proteins form micro-scale vesicles and enter the cytoplasm. These mechanisms will

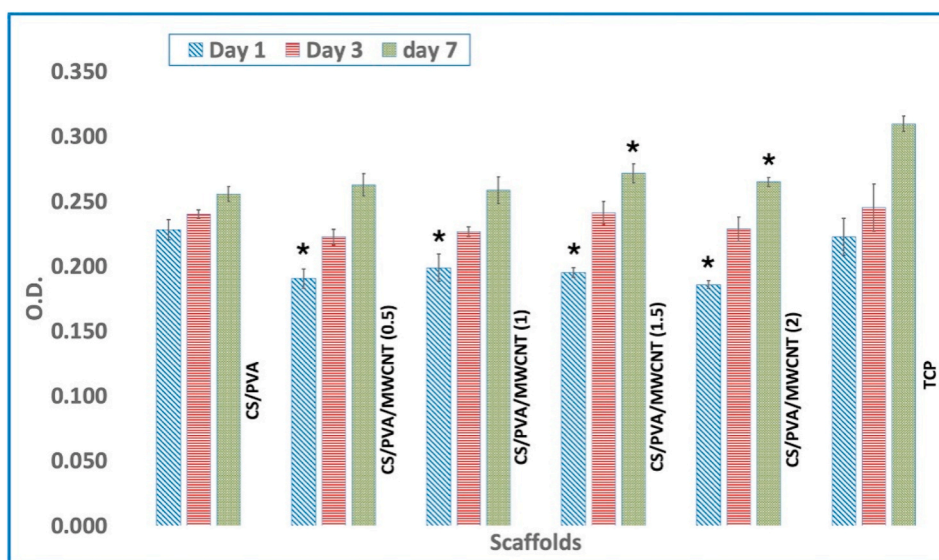


Fig. 7. Cytotoxicity analysis of the effect of fabricated scaffolds on USSCs proliferation by MTT assay. *: p -value less than 0.05; compared to CS/PVA.

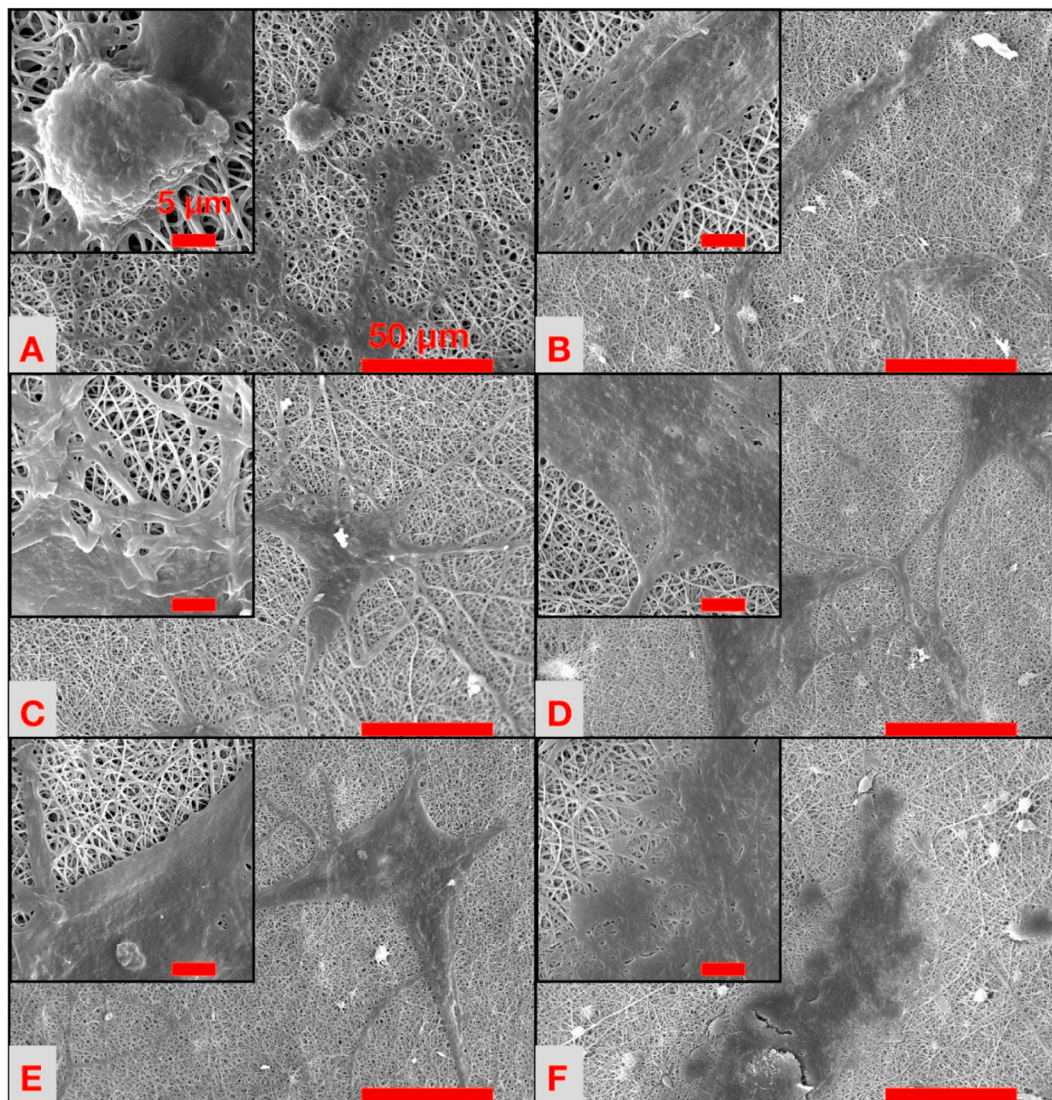


Fig. 8. SEM imaging of cell attachment after 24 h of seeding on fabricated scaffolds: A: CS/PVA, B: CS/PVA/MWCNT (0.5), C: CS/PVA/MWCNT (1), D: CS/PVA/MWCNT (1.5), E: CS/PVA/MWCNT (2), F: CS/PVA/MWCNT (2.5). Scale bars in large and small images equal to 50 μm and 5 μm , respectively.

Table 4

Surface topography data of different electrospun scaffolds. S_a : surface roughness, R_a : linear roughness, V_{vv} : Void volume of the valley section, V_{vc} : Void volume of the core section.

Sample	S_a (μm)	R_a (μm)	V_{vv} ($\mu\text{m}^3/\mu\text{m}^2$)	V_{vc} ($\mu\text{m}^3/\mu\text{m}^2$)
CS/PVA	0.345 ± 0.014	0.367 ± 0.055	0.046 ± 0.002	0.531 ± 0.032
CS/PVA/MWCNT (0.5)	0.353 ± 0.018	0.38 ± 0.049	0.053 ± 0.002	0.528 ± 0.037
CS/PVA/MWCNT (1)	0.367 ± 0.021	0.441 ± 0.019	0.05 ± 0.002	0.560 ± 0.037
CS/PVA/MWCNT (1.5)	0.392 ± 0.007	0.378 ± 0.025	0.063 ± 0.002	0.563 ± 0.006
CS/PVA/MWCNT (2)	0.431 ± 0.04	0.55 ± 0.081	0.057 ± 0.004	0.647 ± 0.078

cause the expression of inflammation and apoptotic factors along with the disruption of the cell membrane. In this regard, the largest colonies (1949 nm in diameter) of MWCNTs in RPMI form from 40 $\mu\text{g}/\text{mL}$ carboxyl-functionalized MWCNTs [65]. TEM has shown that A549 cells have formed vesicles of up to 5 μm of MWCNTs in the first 24 h of

culture, which has resulted in a decrease in viability by 30%. This occurred along with a 10% increase in lactate dehydrogenase (LDH) (and change in IL-8, IL-6, and TNF α levels by 2.5, 10, and 70-times compared to control samples, respectively [65]. Yan et al. showed that in 72 h of a culture of ARPE-19 cells on scaffolds containing 50 $\mu\text{g}/\text{mL}$ MWCNT-COOH, the levels of LDH and ROS were increased by 2 and 3-times, respectively, although cell spreading is normal. Meanwhile, caspase expression, which is related to apoptosis, was raised by 20-times [66]. This is following our results on the lower cell survival in the first 24 h of culture on scaffolds containing MWCNTs.

After 3 days, MWCNTs-containing scaffolds show better cell support, where cell numbers on CS/PVA/MWCNT (1.5) and CS/PVA/MWCNT (2) are equal to CS/PVA samples. At day 7, CS/PVA/MWCNT (1.5) and CS/PVA/MWCNT (2) samples show better support for cell growth compare to CS/PVA. Considering a doubling time of 48 h for USSCs, it shows that after the attachment phase, where a large number of cells do not survive due to stress, MWCNTs-containing samples have better support for growth as compared to CS/PVA samples.

The lower diameter of fibers, higher surface area, and electrical conductivity of MWCNTs-containing scaffolds have eased cell signaling and forces cells to form cellular extensions [9]. Interaction between actin filaments and laminin on the surface of scaffolds will help form

these cellular extensions, or filopodia, which is shown in SEM images in Fig. 8 [63]. Liao et al. have shown that fibroblasts cultured on CS/PVA scaffolds with 1 wt% MWCNTs exhibited the different morphology of forming polygonal shape after 8 h and connections with other cells; whereas on control samples, spindle shaped cells with poor connections were observed [16]. This is in accordance with our results on cell spreading on CS/PVA/MWCNT (2), where cells have formed polygonal shapes with cellular extensions growing in all directions, whereas on CS/PVA samples, cells have shown limited outgrowth of cellular extensions (Fig. 8).

Porosity volume (V_{vv}) can be another influential factor in attachment and cell spreading, which is 24% larger in CS/PVA/MWCNT (2) scaffolds as compared to CS/PVA scaffolds (Table 4). Another factor that can promote the attachment and growth of cells is the homogenous distribution of MWCNTs. These particles are 10–100 nm in diameter, and their formation inside nanofibers can be very similar to the native pattern of cardiac tissue ECM, which consists of networks of entangled elastin and collagen ranging between 10 and 300 nm in diameter [62]. Furthermore, MWCNTs have cylindrical structures with hydrophilic characteristics, which may enable them to entrap proteins [16].

Protein absorption at the scaffold surface can affect the behavior and reaction of cells [67]. [Chang, 2011 #75] Therefore, the homogeneous distribution of these particles can promote cell growth and migration. In a similar study, MWCNTs-containing CS/PVA scaffolds were able to absorb serum proteins by 17%, whereas CS/PVA scaffolds absorbed only 13% of serum proteins; this resulted in a 20% increase in cell viability on CS/PVA/MWCNT scaffolds in day 7 [16]. Overall, we can conclude that scaffolds with up to 2 wt% MWCNTs demonstrate more surface area, electroconductivity and roughness, and a better support for cell survival and growth. Therefore, the CS/PVA/MWCNT (2) scaffolds were selected for our further steps.

3.7. Cardiac differentiation and gene expression

Gene expression analysis was performed using qPCR on day 12, and data was extracted using Rotor Gene Q and interpreted using Rest 2009 software. In this regard, expression of β -MHC, α -MHC, CX43, and cTnI were studied in different treatments, including: TCP negative control samples, TCP with the induction of small molecules, scaffolds with the induction of small molecules with/without electrical stimulation

(Table 2). It is worth mentioning that α -MHC was not expressed in different samples in 40 cycles of qPCR. The remaining three genes, CX43, β -MHC, and cTnI, are related to proteins responsible for contractile function in adult cardiac cells.

As shown in Fig. 9, samples with the induction of both small molecules, and electrical stimulation (Scaffold + SM + ES) show a significant increase in the expression of CX43, β -MHC, and cTnI, 5.3, 64, and 172-times as normalized to undifferentiated cells, respectively (p -values ≤ 0.05). However, in TCP samples induced with only small molecules, expression of β -MHC and cTnI is 2 and 2.3-times the control samples (p -values ≤ 0.05). On scaffold samples, induction of small molecules results in expression of β -MHC and cTnI by 3.1 and 58-times more (p -values ≤ 0.05).

Small molecules are the crucial factors in determining the level of cardiac control of Wnt/beta-catenin, TGF- β and SHH pathways. 5-Azacytidine, as a chemical analogue of cytidine, is commonly known as a demethylation pharmaceutical that can induce MSCs into cardiomyocyte-like cells. Treatment of cells with this agent for 24 h may be effective for cardiac differentiation and generating spindle-shaped morphology [68,69]. As shown in Fig. 10, in our research, the shape of the treated cells turned into spindle-like cells during induction.

5-azacytidine leads to cardiac differentiation via increasing glycogen synthase kinase-3beta (GSK-3beta) expression. GSK-3beta is involved in the regulation and phosphorylation of the Wnt/beta-catenin signaling pathway [68]. A similar study also showed MSCs treatment with 5-azacytidine for cardiac differentiation, which resulted in morphological changes into spindle-shaped cells that steadily enlarged in size during 5-azacytidine induction, along with primitive myofilaments growth [69].

By the end of day 1, CHIR is added to the media, activating Wnt/beta-catenin signaling, which likely pushes cells into mesoendoderm lineage [28,70,71]. Afterward, by the end of day 2, IWP2 is added to the differentiation media, which disables the Wnt/beta-catenin pathway in order to suppress the biphasic behavior of this pathway [28]. The Wnt signaling pathway plays a vital role in the early stages of cardiomyocyte differentiation and later acts as a limiting factor. This biphasic behavior of Wnt has been observed in both mesenchymal and pluripotent stem cells [28,72]. Then, SB431542, by controlling the TGF- β receptor and Purmorphamine, as the SHH receptor agonists, stimulate SHH receptor and suppress cell growth, which may generate cardiac progenitor cells

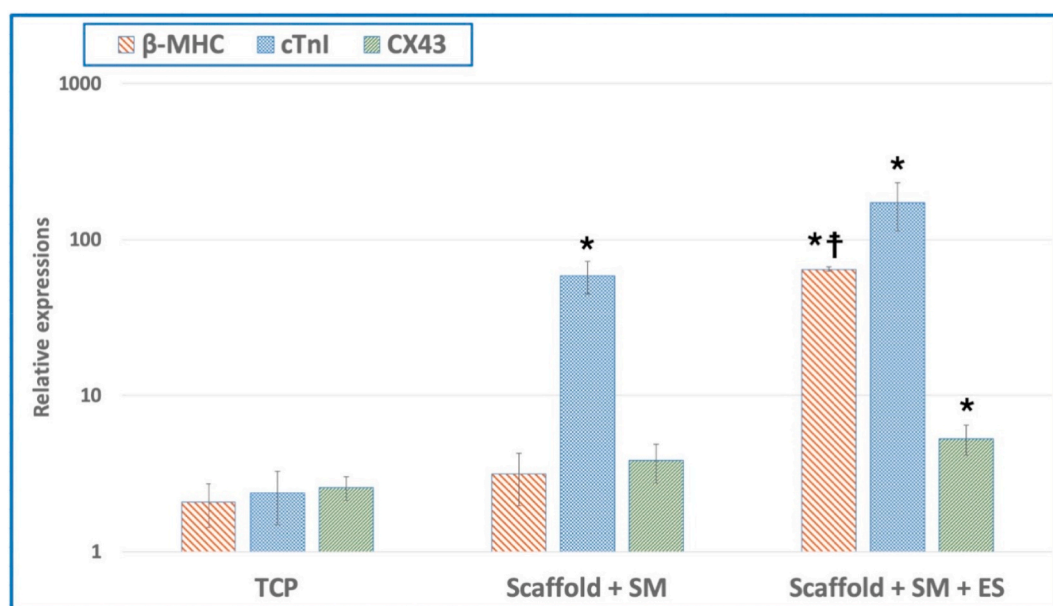


Fig. 9. Expression pattern of cardiac-associated genes in our different experimental groups. *: p -value less than 0.05 compared to the TCP values (). †: p -value less than 0.05 in Scaffold + SM + ES samples compared to Scaffold + SM samples. SM: small molecules, ES: electrical stimulation.

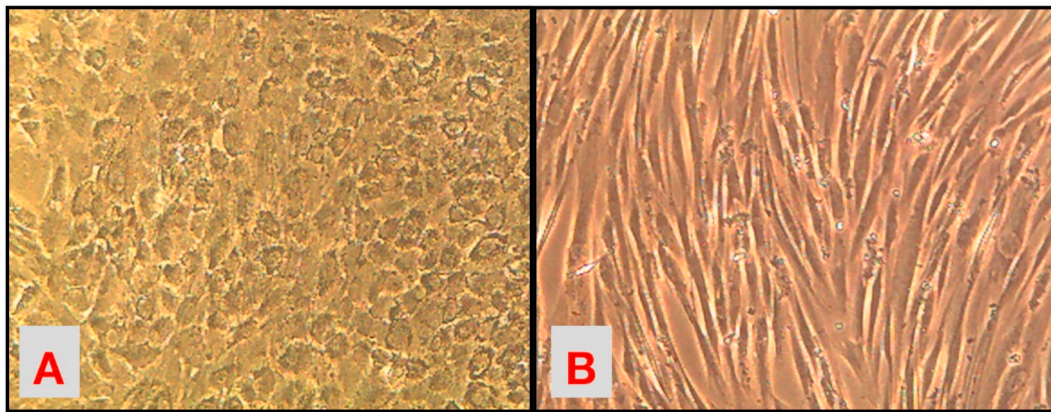


Fig. 10. Light microscopy images of USSCs cultured on TCPs at day 8, without induction of differentiation (A), and with induction of differentiation (B). Both images presented at 100 × magnification.

[28]. In this respect, Felicia Ng et al. showed that the usage of the SB431542 was effective in inactivating the TGF- β pathway and decreased the growth and proliferation of MSCs [73].

In the end, electrical stimulation enhances intracellular activities, including calcium handling, phosphatase and transcription factor activation, and protein kinase expression and activation. Electrical stimulation by activating the CaMK (Ca^{2+} /calmodulin-dependent protein kinase) channel, leads to the creation of calcium handling and oxidative stress. Activation of CaMK-I and CaMK-IV will activate phosphatases, like calcineurin, which will help the maturation of cardiac cells and potentially cause hypertrophy [74].

On the other hand, oxidative stress can act as a secondary messenger in cells and activate the cascades of signaling pathways related to growth and differentiation [75]. Another advantage of using electrical stimulation and conductive scaffolds is an arrangement of cells that will promote proper signal and electrical transfer [9]. Also, electrical stimulation will cause depolarization of cell membranes and form action-potential, which in turn result in the activation of cellular receptors and redistribution of ions. Factors such as the formation of action-potential and redistribution of ions like calcium are essential in maturation of cardiac cells, and these factors are mainly governed by three families of proteins CXs, Troponins, and MHCs [74]. In this research, three genes of these families have been observed to significantly upregulate using combination of small molecules and electrical stimulation. The latter is shown through qPCR analysis, as well as alternation in the morphology of the cells. An increase in expression of these genes enhances the formation of elongated spindle-shaped cells, which confirmed the cardiac differentiation of USSCs.

4. Conclusions

Challenges in engineering the cardiac tissue depend on multiple aspects, including fabrication of conductive scaffolds, choosing a good source of stem cells, and selection of a proper differentiation protocol to reach maturation of cardiac tissues *in vitro*. In this study, we applied all these aspects to mimic the natural environment of cardiac tissue. MWCNTs-containing CS/PVA scaffolds were optimized in terms of electrical conductivity, mechanical properties, morphology, and topological features. USSCs, which were previously reported to be potent for differentiation into various lineages, were cultured on these scaffolds. Additionally, differentiation protocol using small molecules and electrical stimulation was used to push cells into the right path of differentiation, which finally led to the upregulation of cardiac-related genes. This research shows the importance of the simultaneous implementation of different factors in differentiation. In fact, each of the mentioned factors is crucial in developing more efficient and functional cardiac tissue *in vitro*. Altogether, it is recommended to deploy all these factors,

including conductivity of scaffolds, electrical stimulation, and chemical differentiation factors, in order to reach a successful method of engineering cardiac tissue.

Funding

The authors received no specific funding for this work.

Ethical approval

All applicable international, national, and/or institutional guidelines for the care and use of animals were followed.

CRediT authorship contribution statement

Ali Abedi: Conceptualization, Conception and design of study, Funding acquisition, acquisition of, Data curation, data, Formal analysis, analysis and/or interpretation of data, Writing - original draft, Drafting the manuscript, Approval of the version of the manuscript to be published. **Behnaz Bakhshandeh:** Conceptualization, Conception and design of study, Formal analysis, analysis and/or interpretation of, Data curation, data, Writing - original draft, Drafting the manuscript, Approval of the version of the manuscript to be published. **Ali Babaie:** Conceptualization, Conception and design of study, Funding acquisition, acquisition of, Data curation, data, Formal analysis, analysis and/or interpretation of data, Writing - original draft, Drafting the manuscript, Approval of the version of the manuscript to be published. **Javad Mohammadnejad:** Conceptualization, Conception and design of study, Formal analysis, analysis and/or interpretation of, Data curation, data, revising the manuscript critically for important intellectual content, Approval of the version of the manuscript to be published. **Sadaf Vahdat:** Formal analysis, analysis and/or interpretation of, Data curation, data, revising the manuscript critically for important intellectual content, Approval of the version of the manuscript to be published. **Reza Mombeiny:** Formal analysis, analysis and/or interpretation of, Data curation, data, revising the manuscript critically for important intellectual content, Approval of the version of the manuscript to be published. **Seyed Reza Moosavi:** Formal analysis, analysis and/or interpretation of, Data curation, data, revising the manuscript critically for important intellectual content, Approval of the version of the manuscript to be published. **Javid Amini:** analysis and/or interpretation of, Data curation, data, revising the manuscript critically for important intellectual content, Approval of the version of the manuscript to be published. **Lobat Tayebi:** Formal analysis, analysis and/or interpretation of, Data curation, data, revising the manuscript critically for important intellectual content, Approval of the version of the manuscript to be published.

Declaration of competing interest

The authors declare that they have no known competing financial interests or personal relationships that could have appeared to influence the work reported in this paper.

Appendix A. Supplementary data

Supplementary data to this article can be found online at <https://doi.org/10.1016/j.matchemphys.2020.123842>.

References

- [1] R. Chaudhuri, et al., Biomaterials and cells for cardiac tissue engineering: current choices, *Mater. Sci. Eng. C*. 79 (2017) 950–957.
- [2] M. Rasekhi, et al., A novel protocol to provide a suitable cardiac model from induced pluripotent stem cells, *Biol. 50* (2017) 42–48.
- [3] S. Kaptoge, et al., World Health Organization cardiovascular disease risk charts: revised models to estimate risk in 21 global regions, *The Lanc. Glob. Health*. 7 (10) (2019) e1332–e1345.
- [4] V. Bhaathary, et al., Biologically improved nanofibrous scaffolds for cardiac tissue engineering, *Mater. Sci. Eng. C*. 44 (2014) 268–277.
- [5] M.P. Prabhakaran, et al., Biomimetic material strategies for cardiac tissue engineering, *Mater. Sci. Eng. C*. 31 (3) (2011) 503–513.
- [6] B. Bakhshandeh, et al., Tissue engineering: strategies, tissues, and biomaterials, *Biotechnol. Genet. Eng. Rev.* 33 (2) (2017) 144–172.
- [7] S. Hosseinzadeh, et al., Polyethylenimine: a new differentiation factor to endothelial/cardiac tissue, *J. Cell. Biochem.* 120 (2) (2018) 1511–1521.
- [8] S. Abdulghani, G.R. Mitchell, Biomaterials for in situ tissue regeneration: a review, *Biomol.* 9 (11) (2019) 750.
- [9] A. Abedi, M. Hasanzadeh, L. Tayebi, Conductive nanofibrous Chitosan/PEDOT: PSS tissue engineering scaffolds, *Mater. Chem. Phys.* 237 (2019) 121882.
- [10] N. Adadi, et al., Electrospun fibrous PVDF-TrFe scaffolds for cardiac tissue engineering, differentiation, and maturation, *Adv. Mater. Technol.* 5 (3) (2020), 1900820.
- [11] T. Hoshiba, et al., Decellularized matrices for tissue engineering, *Exp. Opin. Biol. Ther.* 10 (12) (2010) 1717–1728.
- [12] S. Hosseinzadeh, et al., Mucoadhesive nanofibrous membrane with anti-inflammatory activity, *Polym. Bull.* 76 (9) (2019) 4827–4840.
- [13] P.-H. Kim, J.-Y. Cho, Myocardial tissue engineering using electrospun nanofiber composites, *BMB Rep.* 49 (1) (2016) 26.
- [14] K. Kalishwaralal, et al., A novel biocompatible chitosan–Selenium nanoparticles (SeNPs) film with electrical conductivity for cardiac tissue engineering application, *Mater. Sci. Eng. C*. 92 (2018) 151–160.
- [15] B.S. Harrison, A. Atala, Carbon nanotube applications for tissue engineering, *Biomater.* 28 (2) (2007) 344–353.
- [16] H. Liao, et al., Improved cellular response on multiwalled carbon nanotube-incorporated electrospun polyvinyl alcohol/chitosan nanofibrous scaffolds, *Col. Surf. B Biointer.* 84 (2) (2011) 528–535.
- [17] M.D. Dozois, et al., Carbon nanomaterial-enhanced scaffolds for the creation of cardiac tissue constructs: a new frontier in cardiac tissue engineering, *Carb.* 120 (2017) 338–349.
- [18] S.S.E. Bakhtiari, et al., Chitosan/MWCNTs composite as bone substitute: physical, mechanical, bioactivity, and biodegradation evaluation, *Polym. Compos.* 40 (S2) (2019) E1622–E1632.
- [19] S. Mombini, et al., Chitosan-PVA-CNT nanofibers as electrically conductive scaffolds for cardiovascular tissue engineering, *Int. J. Biol. Macromol.* 140 (2019) 278–287.
- [20] B. Gorain, et al., Carbon nanotube scaffolds as emerging nanoplatform for myocardial tissue regeneration: a review of recent developments and therapeutic implications, *Biomed. Pharmacother.* 104 (2018) 496–508.
- [21] Z. Chen, X. Mo, F. Qing, Electrospinning of collagen–chitosan complex, *Mater. Lett.* 61 (16) (2007) 3490–3494.
- [22] B. Duan, et al., Electrospinning of chitosan solutions in acetic acid with poly (ethylene oxide), *J. Biomater. Sci. Polym. Ed.* 15 (6) (2004) 797–811.
- [23] B. Son, et al., Antibacterial electrospun chitosan/poly (vinyl alcohol) nanofibers containing silver nitrate and titanium dioxide, *J. Appl. Polym. Sci.* 111 (6) (2009) 2892–2899.
- [24] M.O. Oftadeh, et al., Sequential application of mineralized electroconductive scaffold and electrical stimulation for efficient osteogenesis, *J. Biomed. Mater. Res.* 106 (5) (2018) 1200–1210.
- [25] L. Ghasemi-Mobarakeh, et al., Application of conductive polymers, scaffolds and electrical stimulation for nerve tissue engineering, *J. of Tiss. Eng. and Regen.* 5 (4) (2011) e17–e35.
- [26] M.N. Hirt, et al., Functional improvement and maturation of rat and human engineered heart tissue by chronic electrical stimulation, *J. Mol. Cell. Cardiol.* 74 (2014) 151–161.
- [27] N. Tandon, et al., Optimization of electrical stimulation parameters for cardiac tissue engineering, *J. of Tiss. Eng. and Regen.* 5 (6) (2011) e115–e125.
- [28] H. Fonoudi, et al., A universal and robust integrated platform for the scalable production of human cardiomyocytes from pluripotent stem cells, *Stem Cell. Trans. Med.* 4 (12) (2015) 1482–1494.
- [29] J. Leor, Y. Amsalem, S. Cohen, Cells, scaffolds, and molecules for myocardial tissue engineering, *Pharmacol. & Therap.* 105 (2) (2005) 151–163.
- [30] S. Santourlidis, et al., Unrestricted somatic stem cells (USSC) from human umbilical cord blood display uncommitted epigenetic signatures of the major stem cell pluripotency genes, *Stem Cell. Res.* 6 (1) (2011) 60–69.
- [31] J. Schira, et al., Characterization of regenerative phenotype of unrestricted somatic stem cells (USSC) from human umbilical cord blood (hUCB) by functional secretome analysis, *Mol. Cell. Proteomics* 14 (10) (2015) 2630–2643.
- [32] B. Bakhshandeh, et al., Effective combination of aligned nanocomposite nanofibers and human unrestricted somatic stem cells for bone tissue engineering, *Acta Pharmacol. Sin.* 32 (5) (2011) 626–636.
- [33] L. Ghasemi-Mobarakeh, D. Semnani, M. Morshed, A novel method for porosity measurement of various surface layers of nanofibers mat using image analysis for tissue engineering applications, *J. Appl. Polym. Sci.* 106 (4) (2007) 2536–2542.
- [34] A. Baji, et al., Electrospinning of polymer nanofibers: effects on oriented morphology, structures and tensile properties, *Compos. Sci. Technol.* 70 (5) (2010) 703–718.
- [35] Y. Li, Z. Huang, Y. Lü, Electrospinning of nylon-6, 66, 1010 terpolymer, *Eur. Polym. J.* 42 (7) (2006) 1696–1704.
- [36] M.C. McManus, et al., Mechanical properties of electrospun fibrinogen structures, *Acta Biomater.* 2 (1) (2006) 19–28.
- [37] K. Narttamrongtutt, G.G. Chase, The influence of salt and solvent concentrations on electrospun polyvinylpyrrolidone fiber diameters and bead formation, *Polym.* 54 (8) (2013) 2166–2173.
- [38] P. Lu, Y.-L. Hsieh, Multiwalled carbon nanotube (MWCNT) reinforced cellulose fibers by electrospinning, *ACS Appl. Mater. & Inter.* 2 (8) (2010) 2413–2420.
- [39] M. Omastová, E. Číková, M. Mičušík, Electrospinning of ethylene vinyl acetate/carbon nanotube nanocomposite fibers, *Polym.* 11 (3) (2019) 550.
- [40] M.A. Abureesh, A.A. Oladipo, M. Gazi, Facile synthesis of glucose-sensitive chitosan–poly (vinyl alcohol) hydrogel: drug release optimization and swelling properties, *Int. J. Biol. Macromol.* 90 (2016) 75–80.
- [41] E.A. El-Hefian, M.M. Nasef, A.H. Yahaya, The preparation and characterization of chitosan/poly (vinyl alcohol) blended films, *J. Chem.* 7 (4) (2010) 1212–1219.
- [42] M. Fernandes Queiroz, et al., Does the use of chitosan contribute to oxalate kidney stone formation? *Mar. Drug.* 13 (1) (2015) 141–158.
- [43] A. Misra, et al., FTIR studies of nitrogen doped carbon nanotubes, *Diam. Relat. Mater.* 15 (2–3) (2006) 385–388.
- [44] R.B. Patel, et al., Boron-filled hybrid carbon nanotubes, *Sci. Rep.* 6 (2016) 30495.
- [45] F. Navarro-Pardo, A.L. Martinez-Hernandez, C. Velasco-Santos, Carbon nanotube and graphene based polyamide electrospun nanocomposites: a review, *J. Nanomater.* (2016), 3182761, 2016.
- [46] J. Venkatesan, S.-K. Kim, Chitosan composites for bone tissue engineering—an overview, *Mar. Drug.* 8 (8) (2010) 2252–2266.
- [47] H. Jafari, M. Shahrousvand, B. Kaffashi, Preparation and characterization of reinforced poly (ε-caprolactone) nanocomposites by cellulose nanowhiskers, *Polym. Compos.* 41 (2) (2020) 624–632.
- [48] H. Jafari, M. Shahrousvand, B. Kaffashi, Reinforced poly (ε-caprolactone) bimodal foams via phospho-calcified cellulose nanowhisker for osteogenic differentiation of human mesenchymal stem cells, *ACS Biomater. Sci. Eng.* 4 (7) (2018) 2484–2493.
- [49] A. Aryaei, A.H. Jayatissa, A.C. Jayasuriya, Mechanical and biological properties of chitosan/carbon nanotube nanocomposite films, *J. Biomed. Mater. Res.* 102 (8) (2014) 2704–2712.
- [50] L. Dai, J. Sun, Mechanical Properties of Carbon Nanotubes-Polymer Composites. Carbon Nanotubes—Current Progress of Their Polymer Composites, InTechOpen, 2016, pp. 155–194.
- [51] M. Tavakoli, S. Karbasi, S. Soleymani Eil Bakhtiari, Evaluation of physical, mechanical, and biodegradation of chitosan/graphene oxide composite as bone substitutes, *Polym. Plast. Technol. and Mater.* 59 (4) (2020) 430–440.
- [52] P. AgilAbrahama, V. Rejinib, Preparation of chitosan-polyvinyl alcohol blends and studies on thermal and mechanical properties, *Proced. Technol.* 24 (2016) 741–748.
- [53] G. Kaur, et al., Electrically conductive polymers and composites for biomedical applications, *RSC Adv.* 5 (47) (2015) 37553–37567.
- [54] T.H. Qazi, et al., Development and characterization of novel electrically conductive PANI-PGS composites for cardiac tissue engineering applications, *Acta Biomater.* 10 (6) (2014) 2434–2445.
- [55] D.A. Stout, et al., Mechanisms of greater cardiomyocyte functions on conductive nanoengineered composites for cardiovascular application, *Int. J. Nanomed.* 7 (2012) 5653.
- [56] J. Ma, et al., Role of oxygen-containing groups on MWCNTs in enhanced separation and permeability performance for PVDF hybrid ultrafiltration membranes, *Desal.* 320 (2013) 1–9.
- [57] S. Majeed, et al., Multi-walled carbon nanotubes (MWCNTs) mixed polyacrylonitrile (PAN) ultrafiltration membranes, *J. Membr. Sci.* 403 (2012) 101–109.
- [58] C. Tang, et al., Wet-grinding assisted ultrasonic dispersion of pristine multi-walled carbon nanotubes (MWCNTs) in chitosan solution, *Colloids Surf. B Biointer.* 86 (1) (2011) 189–197.
- [59] S. Han, et al., The wettability and numerical model of different silicon microstructural surfaces, *Appl. Sci.* 9 (3) (2019) 566.
- [60] M.A. Hubbe, D.J. Gardner, W. Shen, Contact angles and wettability of cellulosic surfaces: a review of proposed mechanisms and test strategies, *Biores.* 10 (4) (2015) 8657–8749.
- [61] X. Wang, Q. Zhang, Insight into the influence of surface roughness on the wettability of apatite and dolomite, *Miner.* 10 (2) (2020) 114.

- [62] A. Lobo, et al., An evaluation of cell proliferation and adhesion on vertically-aligned multi-walled carbon nanotube films, *Carb.* 48 (1) (2010) 245–254.
- [63] E. Hirata, et al., Carbon nanotube-coating accelerated cell adhesion and proliferation on poly (L-lactide), *Appl. Surf. Sci.* 262 (2012) 24–27.
- [64] F. Liu, et al., Effect of the porous microstructures of poly (lactic-co-glycolic acid)/carbon nanotube composites on the growth of fibroblast cells, *Soft Mater.* 8 (3) (2010) 239–253.
- [65] C.L. Ursini, et al., Evaluation of uptake, cytotoxicity and inflammatory effects in respiratory cells exposed to pristine and-OH and-COOH functionalized multi-wall carbon nanotubes, *J. Appl. Toxicol.* 36 (3) (2016) 394–403.
- [66] L. Yan, et al., Cytotoxicity and genotoxicity of multi-walled carbon nanotubes with human ocular cells, *Chin. Sci. Bull.* 58 (19) (2013) 2347–2352.
- [67] H.-I. Chang, Y. Wang, Cell responses to surface and architecture of tissue engineering scaffolds, in: *Regenerative Medicine and Tissue Engineering-Cells and Biomaterials*, InTechOpen, 2011.
- [68] Q. Gao, et al., A cocktail method for promoting cardiomyocyte differentiation from bone marrow-derived mesenchymal stem cells, *Stem Cell. Int.* 2014 (2014), 162024.
- [69] Q. Qian, et al., 5-Azacytidine induces cardiac differentiation of human umbilical cord-derived mesenchymal stem cells by activating extracellular regulated kinase, *Stem Cell. Dev.* 21 (1) (2012) 67–75.
- [70] X. Shen, et al., Differentiation of mesenchymal stem cells into cardiomyocytes is regulated by miRNA-1-2 via WNT signaling pathway, *J. Biomed. Sci.* 24 (1) (2017) 29.
- [71] L.-l. Zhang, et al., MiR-499 induces cardiac differentiation of rat mesenchymal stem cells through wnt/ β -catenin signaling pathway, *Biochem. Biophys. Res. Commun.* 420 (4) (2012) 875–881.
- [72] J. Zhang, et al., Yixin-Shu facilitated cardiac-like differentiation of mesenchymal stem cells in vitro, *RSC Adv.* 8 (18) (2018) 10032–10039.
- [73] F. Ng, et al., PDGF, TGF-beta, and FGF signaling is important for differentiation and growth of mesenchymal stem cells (MSCs): transcriptional profiling can identify markers and signaling pathways important in differentiation of MSCs into adipogenic, chondrogenic, and osteogenic lineages, *Blood* 112 (2) (2008) 295–307.
- [74] W.L. Stoppel, D.L. Kaplan, L.D. Black III, Electrical and mechanical stimulation of cardiac cells and tissue constructs, *Adv. Drug Deliv. Rev.* 96 (2016) 135–155.
- [75] E. Serena, et al., Electrical stimulation of human embryonic stem cells: cardiac differentiation and the generation of reactive oxygen species, *Exp. Cell Res.* 315 (20) (2009) 3611–3619.
- [76] A. Babaie, B. Bakhshandeh, A. Abedi, J. Mohammadnejad, I. Shabani, A. Ardehshirylajimi, S.R. Moosavi, J. Amini, L. Tayebi, Synergistic effects of conductive PVA/PEDOT electrospun scaffolds and electrical stimulation for more effective neural tissue engineering, *Eur. Polym. J.* 26 (2020), 110051.